Anisotropic two-dimensional electron gas at $SrTiO_3$(110)

Zhiming Wang[a], Zhicheng Zhong[b], Xianfeng Hao[a], Stefan Gerhold[a], Bernhard Stöger[a], Michael Schmid[a], Jaime Sánchez-Barriga[c], Andrei Varykhalov[c], Cesare Franchini[d], Karsten Held[b], and Ulrike Diebold[a,1]

[a]Institute of Applied Physics, Vienna University of Technology, 1040 Vienna, Austria; [b]Institute of Solid State Physics, Vienna University of Technology, 1040 Vienna, Austria; [c]Helmholtz-Zentrum Berlin, BESSY-II, 12489 Berlin, Germany; and [d]Faculty of Physics and Center for Computational Material Science, University of Vienna, 1090 Vienna, Austria

Edited by Alexis T. Bell, University of California, Berkeley, CA, and approved February 4, 2014 (received for review October 1, 2013)

Two-dimensional electron gases (2DEGs) at oxide heterostructures are attracting considerable attention, as these might one day substitute conventional semiconductors at least for some functionalities. Here we present a minimal setup for such a 2DEG—the $SrTiO_3$(110)-(4 × 1) surface, natively terminated with one monolayer of tetrahedrally coordinated titania. Oxygen vacancies induced by synchrotron radiation migrate underneath this overlayer; this leads to a confining potential and electron doping such that a 2DEG develops. Our angle-resolved photoemission spectroscopy and theoretical results show that confinement along (110) is strikingly different from the (001) crystal orientation. In particular, the quantized subbands show a surprising "semiheavy" band, in contrast with the analog in the bulk, and a high electronic anisotropy. This anisotropy and even the effective mass of the (110) 2DEG is tunable by doping, offering a high flexibility to engineer the properties of this system.

oxide surface | electronic structure | quantum confinement | perovskite | ARPES

The 2D electron gas (2DEG) observed in oxide heterostructures such as $LaAlO_3/SrTiO_3$ (1, 2) offers a possible alternative to conventional semiconductors, not only for electronics at the nanoscale (3) but also because of the possibility of spin-polarized (4) and superconducting (5, 6) currents. An even simpler setup is to create a 2DEG directly at $SrTiO_3$. Recently this was achieved by irradiating a (001) surface (7, 8) with synchrotron radiation, albeit the origin of the resulting 2DEG is still under debate (7–9). This system has two major drawbacks: (*i*) surface oxygen vacancies are very reactive and (*ii*) the (001) surface has no unique surface termination, as TiO_2 and SrO terraces may develop, and the surface structure strongly depends on sample treatment and history (10).

Here, we show that a 2DEG can also be induced at $SrTiO_3$(110), which is stabilized and covered by a reconstructed overlayer. This overlayer automatically forms to compensate the intrinsic polarity of the system. A $SrTiO_3$ crystal can be viewed as a stack of alternating $(SrTiO)^{4+}$ and $(O_2)^{4-}$ planes along the [110] orientation, resulting in a dipole moment that diverges with increasing crystal thickness (11). As is often true for polar surfaces, this is prevented by one of several compensation mechanisms (11). Specifically, the $SrTiO_3$(110) surface spontaneously forms a (4 × 1) reconstruction upon various different sample treatments, including annealing in a tube furnace with flowing high-purity oxygen (12) and standard ultrahigh vacuum preparation procedures (13, 14). The reconstruction consists of a 2D, tetrahedrally coordinated titania overlayer (Fig. 1*A*), which, with a nominal stoichiometry of $(Ti_{1.5}O_4)^{2-}$, quenches the overall dipole moment (12, 15). Because the Ti atoms in the tetrahedral titania surface layer of the reconstruction are saturated by strong, directional bonds, the (4 × 1) surface is chemically quite inert (16).

Results and Discussion

Exposing the $SrTiO_3$(110)-(4 × 1) surface to synchrotron radiation creates oxygen vacancies (V_Os) at the surface (16); they spontaneously migrate beneath the titania overlayer; Fig. 1*A* and *SI Appendix*. The V_O's downward diffusion mechanism is well described by ab initio molecular dynamics (MD) in terms of the concomitant upward diffusion of oxygen atoms from the topmost $(SrTiO)^{4+}$ plane to the surface (see Fig. 1*C* and *SI Appendix*, Figs. S8 and S9 for details). This is a major difference from the $SrTiO_3$(100) surface, where oxygen vacancies remain at the surface; hence in that case the V_Os are not protected by an overlayer and will be filled when oxygen is present at the ambient. The subsurface V_Os at $SrTiO_3$(110) lead to electron doping, and the photoemission spectrum in Fig. 1*D* shows the development of a metallic peak at E_F. Simultaneously, the O 2*p* valence band in Fig. 1*D* shifts to higher binding energy, indicating a downward band bending of ∼0.3 eV (relative to E_F) in the vicinity of the surface. This is in agreement with the density functional theory (DFT+U) (17, 18) calculated potential shown as (layer-resolved) dots in Fig. 1*E*. Note that the topmost titania overlayer has a larger bandgap so that it is not only chemically but also electrically inert.

The pronounced surface potential arising from the downward band banding confines the free charge carriers to a thin layer so that a 2DEG develops beneath the titania overlayer. From our DFT+U calculations we conclude that the charge carriers are localized in the $SrTiO_3$ layers within about 2 nm thickness (Fig. 1*B* and *SI Appendix*, Fig. S12).

We now turn to the unusual properties of the 2DEG at $SrTiO_3$(110)-(4 × 1). Experimentally we identify these from angle-resolved photoemission spectroscopy (ARPES) experiments (see Figs. 3 and 4 below) but for a better understanding we start

Significance

Although still in its infancy, electronics based on all-oxide materials is a rapidly developing field, and strontium titanate is its key player. For this area to thrive, an atomic-scale control and understanding of the materials' surfaces and interfaces needs to be achieved. A $SrTiO_3$ crystal with (110) orientation automatically forms an overlayer that is more insulating than the bulk and chemically less reactive, akin to the native SiO_2 on conventional wafer. With appropriate doping a two-dimensional electron gas (2DEG) forms underneath the $SrTiO_3$(110) surface. This (110) 2DEG is very different from (001): The effective mass here depends on the quantum number, and a completely flat band can be realized. Such a flat band bears good prospects for, among others, magnetism and thermoelectricity.

Author contributions: Z.W. and U.D. designed research; Z.W., Z.Z., X.H., S.G., and B.S. performed research; Z.W., S.G., and B.S. performed experiments; Z.Z. and K.H. performed tight-binding calculations; X.H. and C.F. performed density functional theory calculations; Z.W., M.S., J.S.-B., and A.V. analyzed data; and Z.W., Z.Z., C.F., K.H., and U.D. wrote the paper.

The authors declare no conflict of interest.

This article is a PNAS Direct Submission.

Freely available online through the PNAS open access option.

[1]To whom correspondence should be addressed. E-mail: diebold@iap.tuwien.ac.at.

This article contains supporting information online at www.pnas.org/lookup/suppl/doi:10.1073/pnas.1318304111/-/DCSupplemental.

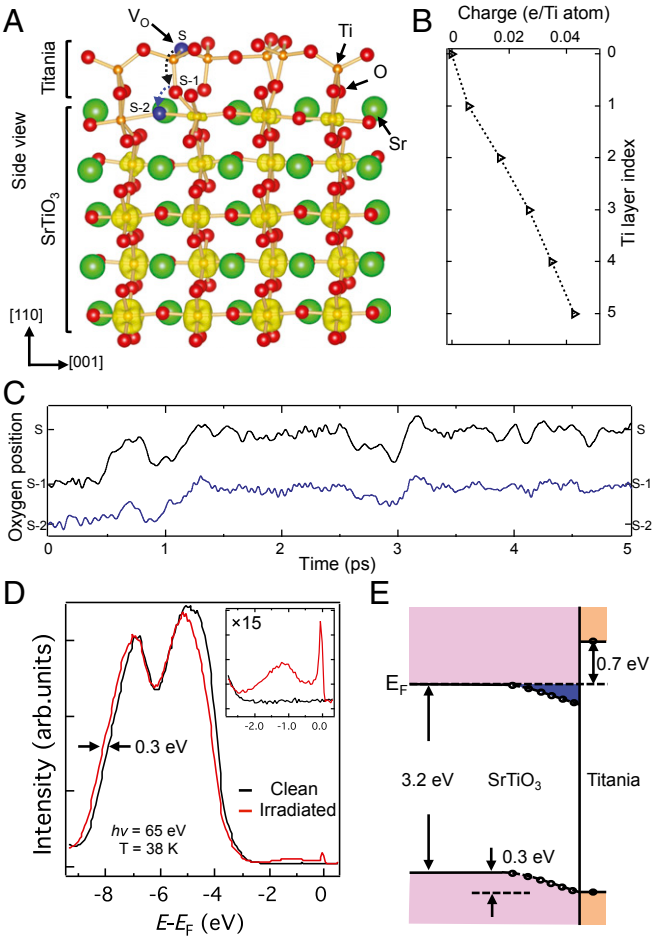

Fig. 1. $SrTiO_3$(110)-(4 × 1) surface. (*A*) Structural model; an oxygen vacancy (V_O) formed at the reconstructed surface spontaneously migrates to the $(SrTiO)^{4+}$ plane beneath the top titania layer. The excess electrons from the V_O form a 2DEG confined within a region of about 2 nm thickness. The layer-dependent charge is represented by the yellow lobes and plotted in *B*. (*C*) MD simulation of the V_O diffusion from the surface (S) to the subsurface (S-2) sites represented by the accompanying upward oxygen migration from S-2 to S-1 (blue line) and from S-1 to S (black line). (*D*) Angle-integrated photoemission spectroscopy of the clean surface and after creating V_Os by synchrotron radiation. An in-gap state and a metallic peak near the Fermi level (E_F) develop (*Inset*). (*E*) Schematic band structure at a surface with V_Os; the bands bend downward by 0.3 eV as deduced from the spectra in *D*. The dots denote the surface potential obtained from the shift of Ti 3*s* states in DFT+U calculations.

with a tight-binding modeling of this 2DEG; the details of the calculations are presented in *SI Appendix*, Sec. S12. In the bulk, $SrTiO_3$ has a gap of 3.2 eV and the three lowest conduction bands are Ti t_{2g} (i.e., d_{xy}, d_{yz}, and d_{zx}; Fig. 2*C*) orbitals that are degenerate at the Γ-point. As the lobes of the d_{yz} orbital point into the *y*–*z* plane (see d_{yz} in Fig. 2*A*), the d_{yz} band has a small hopping amplitude t_2 in the Γ–X direction and is hence weakly dispersive (heavy) along Γ–X. In contrast, d_{xy} and d_{zx} have a larger overlap and hopping amplitude t_1 in this direction, and are thus strongly dispersive (light), as well as degenerate. Along Γ–M, the d_{xy} band is strongly dispersive (light) with hopping amplitude t_1, whereas the d_{yz} and d_{zx} bands are "semilight" with an effective hopping amplitude $(t_1 + t_2)/2$; Fig. 2*C*.

When the t_{2g} electrons are now confined within a few nanometers at the $SrTiO_3$(001) surface, quantum well states (or subbands) are formed. Due to the anisotropy of the t_{2g} orbitals, the level spacing of the quantized subbands strongly depends on the orbital character (7, 19, 20). Notwithstanding, the [001] confinement does not change the carrier properties, i.e., the band dispersion of the subbands stays the same as in the bulk (Fig. 2*D*). In striking contrast, a confinement along the [110] direction modeled with a wedge-shaped potential well (Fig. 1*E*) strongly changes the properties of the carriers, i.e., their band dispersion. As we show in *SI Appendix*, Sec. S12, the effective hopping amplitude of the d_{xy} orbital along the $\overline{\Gamma}-\overline{\mathrm{M}}$ ($[1\bar{1}0]$) direction becomes $t_1\cos(\pi n/(N+1))$, where N is the number of layers and n the quantum number (or subband index). That is, the effective mass of the quantum confined states now depends on the subband index n. For particular values of n, such as $n=2$ in Fig. 2*E*, the dispersion becomes flat. This is also the case for the d_{yz}/d_{zx} orbitals where the quantum confinement leads to an effective hopping amplitude $(2t_1t_2/(t_1+t_2))\cos(\pi n/(N+1))$ along $\overline{\Gamma}-\overline{\mathrm{M}}$. Here, in addition to the quantum number n dependence, the prefactor also changes from its bulk value. As $t_2 \ll t_1$, this prefactor is $\sim 2t_2$ so that the d_{yz}/d_{zx} bands become semiheavy, whereas they are semilight ($\sim t_1/2$; Fig. 2*C*) in the bulk. A simple picture for this semiheavy behavior is that the d_{yz}/d_{zx} electrons are quantum confined along [110] and movement along $[1\bar{1}0]$ requires a zigzag path with hopping amplitude alternating between t_2 and t_1; Fig. 2*B*. Hence only one t_2 hopping is required for moving the electrons by two sites, which explains the effective hopping amplitude $2t_2$.

Fig. 3 shows ARPES results from the $SrTiO_3$(110)-(4 × 1) surface. The measurements were taken along the [001] and $[1\bar{1}0]$ directions. The intensity of the observed bands strongly depends on the light polarization (linear vertical, LV, and linear horizontal). These dichroic effects are due to selection rules (21), and allow disentangling the symmetry and orbital character of the various bands (*SI Appendix*, Figs. S1–S3). This enables us to ascribe the strongly and weakly dispersing bands along the [001] direction to d_{yz}/d_{zx}- and d_{xy}-like orbitals, respectively. Accordingly, the strongly and weakly dispersing bands along the $[1\bar{1}0]$ direction correspond to d_{xy}- and d_{yz}/d_{zx}-like orbitals.

The strongly (weakly) dispersing $d_{yz}/d_{zx}(d_{xy})$-like band along [001] has a bandwidth of ~72 meV (~62 meV) and a Fermi momentum of 0.11 $Å^{-1}$ (0.40 $Å^{-1}$). A fit to a parabolic dispersion yields an effective mass $m^* = 0.67m_e$ (9.7 m_e), with m_e the free electron mass. These [001] effective masses are consistent with those from a 2DEG on the vacuum-fractured $SrTiO_3$(001) surface (7, 8) and the tight-binding description; Table 1. Around the Γ-point the orbital degeneracy is lifted by a splitting of ~10 meV between the d_{yz}/d_{zx}- and d_{xy}-like bands.

From our tight-binding calculations we expect a quite different behavior along the $[1\bar{1}0]$ direction. The $d_{yz}/d_{zx}(d_{xy})$-derived ARPES bands have bandwidths of ~72 meV (62 meV), Fermi momenta of 0.34 $Å^{-1}$ (0.10 $Å^{-1}$), and effective masses of 6.1 (0.74); Fig. 3 *C* and *D*. The former corresponds to a semiheavy band distinct from its semilight behavior in the bulk. In particular, the semiheavy carriers predicted by the tight-binding calculations agree well with the experimental ones; see Table 1 for a summary of the effective masses.

Fig. 3 *E*–*H* shows the second derivatives of the ARPES data along with the corresponding tight-binding subbands dispersion (Fig. 3 *E* and *J*). In addition to the bands discussed above, shallower bands become more visible. These are attributed to d_{yz}/d_{zx}-like subbands, indicating that quantum well states of a 2DEG are formed at $SrTiO_3$(110). The 2D character of the observed bands is further confirmed by the fact that the bands have no dispersion along the [110] direction (surface normal) in photon-energy-dependent measurements (*SI Appendix*, Fig. S4). From the tight-binding calculations we found both d_{yz}/d_{zx}- and d_{xy}-like carriers to be confined within ~2 nm, in excellent agreement with the DFT+U prediction (*SI Appendix*, Figs. S12 and S15).

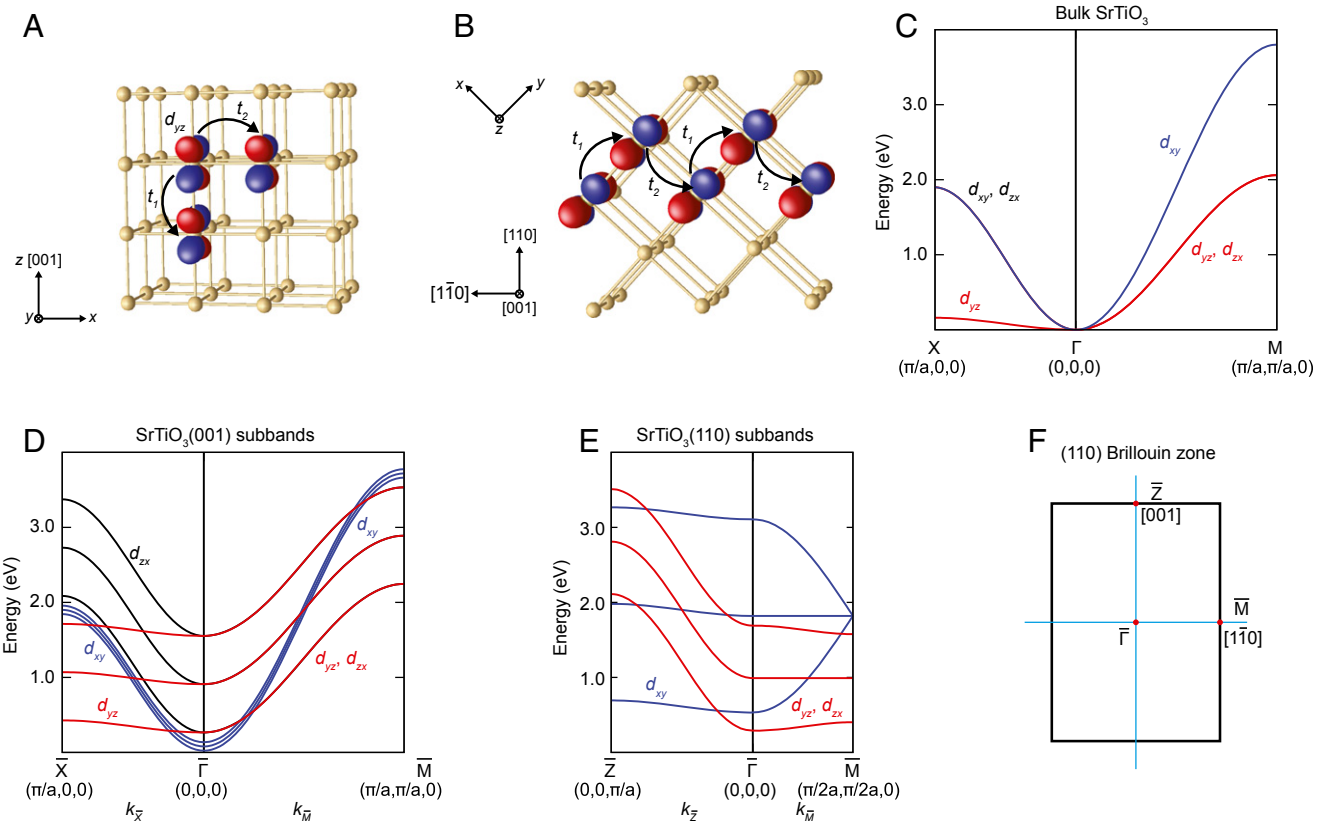

Fig. 2. Effect of quantum confinement on the electronic structure of (001)- and (110)-oriented $SrTiO_3$. (*A* and *B*) Schematics of the Ti lattice in $SrTiO_3$ oriented along the [001] and [110] direction, respectively. Ti $3d_{yz}$ orbital lobes expand in the *y*–*z* plane. Large (t_1) and small (t_2) hopping amplitudes depend on the overlap of the nearest-neighbor *d* orbitals. (*C*) Bulk band structure of $SrTiO_3$, consisting of a heavy d_{yz} band (red) and light d_{xy}/d_{zx} bands (blue) along k_x, as well as a light d_{xy} band (blue) and semilight d_{xy}/d_{zx} bands (red) along k_M. (*D* and *E*) Quantum well states (or subbands) of $SrTiO_3$ confined along the [001] and [110] direction, respectively. The band dispersions of all the quantum well states confined in the (001) direction are the same as in the bulk. Confinement along (110) is different: here the d_{yz}/d_{zx} band becomes semiheavy along the [1$\bar{1}$0] direction and the different (110)-quantum-confined states have a different mass. (*F*) 2D Brillouin zone of the $SrTiO_3$(110) surface.

Fig. 4 shows full photoemission mapping and constant-energy cuts obtained with LV light polarization and detection along the [1$\bar{1}$0] direction. The resulting Fermi surface consists of two perpendicular ellipsoids and a small ellipsoid centered at the Γ-point. The bright (faint) ellipsoid is derived from $d_{yz}/d_{zx}(d_{xy})$-like band and has semiaxes of ~0.11 Å^{-1} (0.4 Å^{-1}) and 0.34 Å^{-1} (0.10 Å^{-1}) along [001] and [1$\bar{1}$0], respectively. From the area (A_F) enclosed by each Fermi surface, the corresponding 2D carrier density is $n_{2D} = A_F/2\pi^2$. Taking into account the three bands that cross E_F, we find 0.39 electrons per 1 × 1 unit cell of $SrTiO_3$(110) (or about 1.8×10^{14} cm^{-2}), a value even larger than the sheet carrier density measured at the bare $SrTiO_3$(100) surface (7, 8).

The Fermi surface measurements further support the conclusion that the 2DEG is not residing at, but underneath, the reconstructed surface layer, as in the former case we would expect a gap opening related to the "4×" periodicity along the [001] direction. Indeed, the Fermi surface lies in the (1 × 1) but not in the reconstructed (4 × 1) Brillouin zone (the latter is indicated by the dashed lines in Fig. 4 *B*–*D*).

Our results explain the dopant-dependent anisotropy at the (110)-oriented $LaAlO_3/SrTiO_3$ interface that was observed recently (22). Although both d_{xy}- and d_{yz}/d_{zx}-derived Fermi surfaces are strongly anisotropic, the difference along the [001] and [1$\bar{1}$0] directions themselves is not very pronounced at higher carrier density, when both ellipsoids are occupied (Fig. 4). However, at a higher binding energy of $E_B = 60$ meV, only the d_{yz}/d_{zx}-derived ellipsoids appears, with a corresponding carrier density of ~1.7×10^{13} cm^{-2}. Remarkably, this is the same carrier density where a pronounced anisotropic conductivity was observed in transport measurements (22). At this doping level, the big difference between the semiheavy and light carriers comes to bear. In the bulk, however, the anisotropy is not so pronounced (see the dashed ellipsoid in Fig. 4*D*).

In conclusion, we have demonstrated that an anisotropic 2DEG can be created on $SrTiO_3$(110). The chemically inert and electrically insulating titania overlayer is native to this system, as it forms spontaneously to lift the intrinsic polarity of this system. It provides for a 2DEG that should be less vulnerable against atmospheric contamination than a 2DEG at the bare surface,

Table 1. Comparisons of experimental and theoretical effective masses of 2DEGs

	$SrTiO_3$(001)		$SrTiO_3$(110)			
	Along $k_{\bar{X}}$		Along $k_{\bar{Z}}$		Along $k_{\bar{M}}$	
Expt. m^*	10~20[†]	0.7[†] 0.5~0.6[‡]	9.7	0.67	6.1	0.74
Theor. m^*	8.2	0.6	8.2	0.6	4.7	0.6
Orbital	d_{yz}	d_{xy}/d_{zx}	d_{xy}	d_{yz}/d_{zx}	d_{yz}/d_{zx}	d_{xy}

The experimental effective masses are slightly larger than those obtained from tight-binding calculations, indicating a minor mass renormalization due to electronic correlations.
[†]Ref. 7.
[‡]Ref. 8.

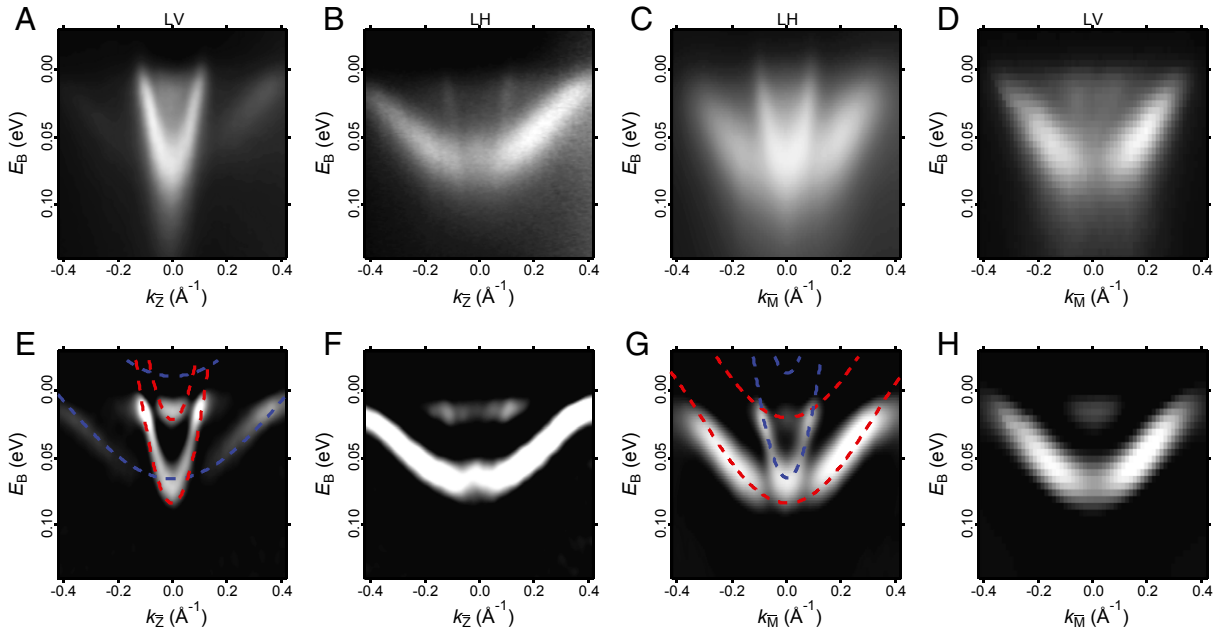

Fig. 3. ARPES of the electronic structure at $SrTiO_3$(110)-(4 × 1). (*A–D*) Energy-momentum intensity maps (T_{sample} = 38 K, $h\nu$ = 65 eV) along the $\bar{\Gamma}-\bar{M}$ (or [001]) direction and the $\bar{\Gamma}-\bar{M}$ (or $[1\bar{1}0]$) direction, respectively. (*E–H*) Corresponding second derivatives. In each direction, the spectra were measured with linear vertical (*A* and *D*) and linear horizontal (*B* and *C*) polarized light. Tight-binding fits are overlaid for both directions. The d_{xy}-like bands are drawn in blue and the d_{yz}/d_{zx}-like bands in red. The d_{xy}-derived bands are weakly dispersive and d_{yz}/d_{zx}-derived bands are strongly dispersive along [001]; the d_{yz}/d_{zx}-derived bands become weakly dispersive and d_{xy}-derived band becomes strongly dispersive along $[1\bar{1}0]$. The subbands become more visible in *E–H*.

and less dependent on the chemical complexity inherent to interfacial 2DEGs. The (110) 2DEG turns out to be strikingly different from the (001) 2DEG, which has been the subject of previous ARPES studies. The band dispersion is not only distinct from the one of the bulk, it even depends on the quantum number for the (110) confinement. Hence one can engineer a completely flat band along $[1\bar{1}0]$, offering good prospects to find exotic properties in the future. For example, as was shown firstly in ref. 23, a flat band naturally leads to so-called "flat-band ferromagnetism," hence offering a route to spin-polarized currents.

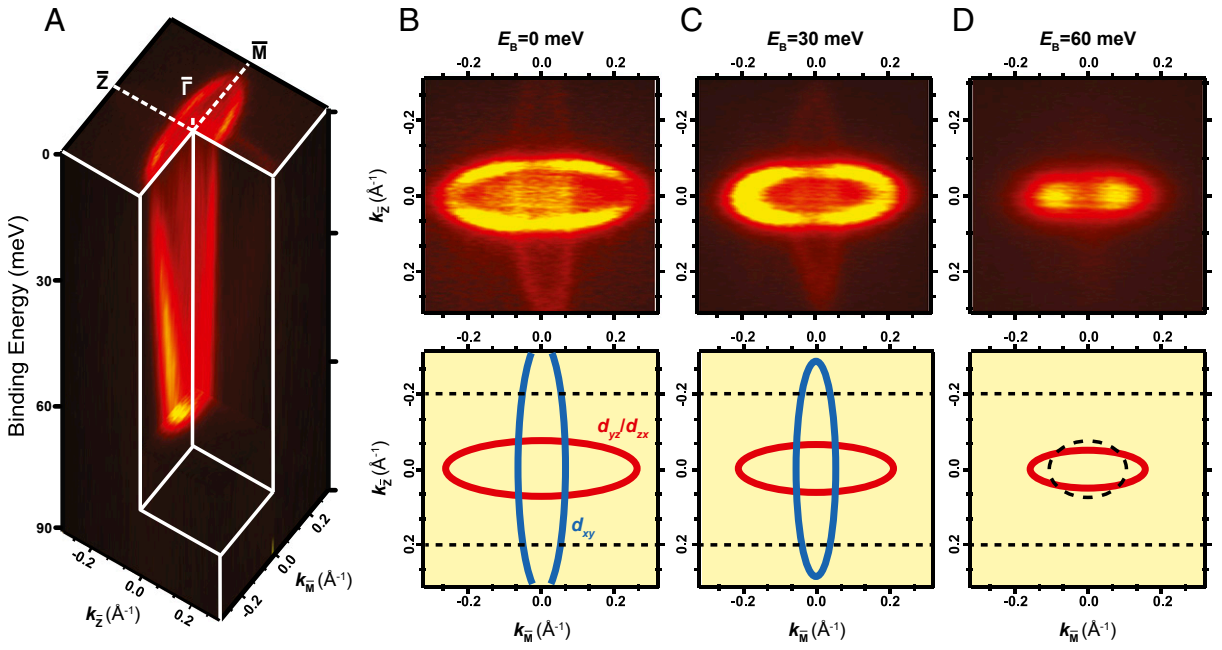

Fig. 4. Overview of the electronic structure. (*A*) Full photoemission mapping and (*B–D*) constant energy cuts at different binding energies (E_B = 0, 30, and 60 meV) and schematic constant-energy surfaces (*Lower*). Data taken with LV light, which emphasizes d_{yz} and d_{zx} orbitals. These appear bright, whereas d_{xy}-derived states appear faint. In the schematics the reconstructed (4 × 1) Brillouin zone is indicated by dotted lines. Note that the Fermi surface lies in the (1 × 1) Brillouin zone, consistent with the 2DEG being confined at the $SrTiO_3$ layers beneath the surface reconstruction. At higher binding energy, E_B = 60 meV, only the d_{yz}/d_{zx}-derived ellipsoid is occupied. The resulting constant-energy surface is strongly anisotropic compared with the bulk projected energy surface (black dashed ellipsoid).

The high density of states associated with the flat band is also advantageous for thermoelectric applications (24) and affects superconducting properties (25). To exploit the flat-band physics as well as the anisotropic features of the (110) 2DEG, a tuning of the carrier density is needed. This is possible in principle by the amount of oxygen vacancies, applying an electric field (26), and the deposition of metal adatoms on the titania overlayer (27). An alternative, more robust way of generating this (110) 2DEG might be a (110)-oriented heterostructure consisting of buried δ-doped La:$SrTiO_3$ layers sandwiched in between undoped $SrTiO_3$ buffer layers.

Materials and Methods

Experiments. The Nb-doped (0.5 wt %) $SrTiO_3$(110) surface was prepared by cycles of Ar^+ sputtering (1 keV, 5 μA, 10 min) followed by annealing in 3×10^{-6} mbar oxygen at 900 °C for 1h. The samples were heated by electron bombardment and the temperature was monitored with an infrared pyrometer. The surface reconstruction was checked by low-energy electron diffraction (LEED) and tuned by depositing Sr metal on the surface, followed by annealing until a sharp (4 × 1) LEED patter was observed (14). The ARPES measurements were performed at the ARPES 1^2 beamline (BESSY II storage ring at the Helmholtz-Zentrum Berlin). All ARPES spectra were recorded using photon energies of 50–70 eV, linearly polarized along the horizontal or vertical direction. A Scienta R8000 analyzer with vertical detection slit geometry was used, with the energy and angular resolution of ∼10 meV and 0.3°, respectively. Sample temperature was at ∼38 K.

Theory. DFT calculations with the inclusion of an effective on-site Coulomb repulsion $U_{eff} = 4.5$ eV for the Ti *d* states were carried out with the Vienna ab initio simulation package, VASP (17, 18), within the projector augmented-wave method and the Perdew–Burke–Ernzerhof functional (28). The computational cell was modeled with a symmetric slab consisting of 45 atomic layers separated by a 12-Å-thick vacuum region. One oxygen vacancy was created on both sides of the symmetrical slab (*SI Appendix*). The kinetic-energy cutoff for the plane-wave expansion was set to 600 eV. We adopted a (4 × 1) 2D unit cell, and a (2 × 3 × 1) Monkhorst–Pack k-point mesh. During the structural optimization, atoms in the central nine layers were kept fixed to the corresponding bulk positions, whereas the other atoms were allowed to relax until the forces on each atom were less than 0.02 eV/Å. The V_O diffusion was studied in a seven-layer-thick slab by means of ab initio canonical molecular dynamics at a simulating temperature of 1000 K for 5 ps, with a time step of 1 fs, using the Nosé thermostat (29).

The hopping parameters for the tight-binding calculations have been obtained both by (*i*) fitting the nearest-neighbor hopping parameters to the DFT bandwidth of bulk $SrTiO_3$ yielding $t_1 = -0.455$ eV and $t_2 = -0.04$ eV, and (*ii*) more thoroughly through a Wannier function projection (30, 31) of a Wien2K (32) DFT calculation, using the generalized gradient approximation (28) and 10 × 10 × 10 *k*-point grid. For further tight-binding calculations, up to next-nearest-neighbor hopping has been taken into account; see *SI Appendix*, Secs. S12 and S13 for details.

ACKNOWLEDGMENTS. Z.W., X.H., and U.D. gratefully acknowledge support by the European Research Council (ERC) Advanced Grant "OxideSurfaces" and the Austrian Science Fund (Fonds zur Förderung der Wissenschaftlichen Forschung, FWF, Project F45). Z.Z. acknowledges support by the FWF through SFB VicOM F41. K.H. acknowledges support by the ERC Starting Grant AbinitioDΓA, Grant Agreement 306447. The DFT computations were performed on the Vienna Scientific Cluster (VSC-2).

1. Mannhart J, Schlom DG (2010) Oxide interfaces—an opportunity for electronics. *Science* 327(5973):1607–1611.
2. Ohtomo A, Hwang HY (2004) A high-mobility electron gas at the $LaAlO_3/SrTiO_3$ heterointerface. *Nature* 427(6973):423–426.
3. Cen C, Thiel S, Mannhart J, Levy J (2009) Oxide nanoelectronics on demand. *Science* 323(5917):1026–1030.
4. Brinkman A, et al. (2007) Magnetic effects at the interface between non-magnetic oxides. *Nat Mater* 6(7):493–496.
5. Thiel S, Hammerl G, Schmehl A, Schneider CW, Mannhart J (2006) Tunable quasi-two-dimensional electron gases in oxide heterostructures. *Science* 313(5795):1942–1945.
6. Reyren N, et al. (2007) Superconducting interfaces between insulating oxides. *Science* 317(5842):1196–1199.
7. Santander-Syro AF, et al. (2011) Two-dimensional electron gas with universal subbands at the surface of $SrTiO_{(3)}$. *Nature* 469(7329):189–193.
8. Meevasana W, et al. (2011) Creation and control of a two-dimensional electron liquid at the bare $SrTiO_3$ surface. *Nat Mater* 10(2):114–118.
9. Plumb NC, et al. (2013) Mixed dimensionality of confined conducting electrons tied to ferroelectric surface distortion on an oxide. arXiv:1302.0708.
10. Bonnell DA, Garra J (2008) Scanning probe microscopy of oxide surfaces: atomic structure and properties. *Rep Prog Phys* 71(4):044501-1–044501-27.
11. Goniakowski J, Finocchi F, Noguera C (2008) Polarity of oxide surfaces and nanostructures. *Rep Prog Phys* 71(1):016501-1–016501-55.
12. Enterkin JA, et al. (2010) A homologous series of structures on the surface of $SrTiO_3$(110). *Nat Mater* 9(3):245–248.
13. Russell B, Castell M (2008) Reconstructions on the polar $SrTiO_3$(110) surface: Analysis using STM, LEED and AES. *Phys Rev B* 77(24):245414-1–245414-9.
14. Wang Z, et al. (2011) Evolution of the surface structures on $SrTiO_3$(110) tuned by Ti or Sr concentration. *Phys Rev B* 83(15):155453-1–155454-9.
15. Li F, et al. (2011) Reversible transition between thermodynamically stable phases with low density of oxygen vacancies on the $SrTiO_3$(110) surface. *Phys Rev Lett* 107(3): 036103-1–036103-4.
16. Wang Z, et al. (2013) Water adsorption at the tetrahedra titania surface layer of $SrTiO_3$(110)-(4×1). *J Phys Chem C* 117(49):26060–26069.
17. Kresse G, Hafner J (1993) *Ab initio* molecular dynamics for open-shell transition metals. *Phys Rev B Condens Matter* 48(17):13115–13118.
18. Kresse G, Furthmüller J (1996) Efficiency of *ab-initio* total energy calculations for metals and semiconductors using a plane-wave basis set. *Comput Mater Sci* 6(1):15–50.
19. Yoshimatsu K, et al. (2011) Metallic quantum well states in artificial structures of strongly correlated oxide. *Science* 333(6040):319–322.
20. Zhong Z, Zhang Q, Held K (2013) Quantum confinement in perovskite oxide heterostructures: Tight binding instead of a nearly free electron picture. *Phys Rev B* 88(12): 125401-1–125401-8.
21. Aiura Y, et al. (2002) Photoemission study of the metallic state of lightly electron-doped $SrTiO_3$. *Surf Sci* 515(1):61–74.
22. Annadi A, et al. (2013) Anisotropic two-dimensional electron gas at the $LaAlO_3/SrTiO_3$(110) interface. *Nat Comm* 4:1838-1–1838-7.
23. Mielke A, Tasaki H (1993) Ferromagnetism in the Hubbard model. *Commun Math Phys* 158(2):341–371.
24. Mahan G, Sales B, Sharp J (1997) Thermoelectric materials: New approaches to an old problem. *Phys Today* 50(3):42–47.
25. Herranz G, Bergeal N, Lesueur J, Gazquez J (2013) Orientational tuning of the 2D-superconductivity in LaAlO3/SrTiO3 interfaces. arXiv:1305.2411.
26. Ueno K, et al. (2008) Electric-field-induced superconductivity in an insulator. *Nat Mater* 7(11):855–858.
27. Wang Z, et al. (2013) Strain-induced defect superstructure on the $SrTiO_3$(110) surface. *Phys Rev Lett* 111(5):056101-1–056101-5.
28. Perdew JP, Burke K, Ernzerhof M (1996) Generalized gradient approximation made simple. *Phys Rev Lett* 77(18):3865–3868.
29. Nosé S (1984) A unified formulation of the constant temperature molecular dynamics methods. *J Chem Phys* 81(1):511–519.
30. Kuneš J, et al. (2010) Wien2wannier: From linearized augmented plane waves to maximally localized Wannier functions. *Comput Phys Commun* 181(11):1888–1895.
31. Mostofi AA, et al. (2008) Wannier90: A tool for obtaining maximally-localised Wannier functions. *Comput Phys Commun* 178(9):685–699.
32. Blaha P, Schwarz K, Madsen GKH, Kvasnicka D, Luitz J (2001) WIEN2k, An Augmented Plane Wave + Local Orbitals Program for Calculating Crystal Properties (Karlheinz Schwarz, Vienna Univ of Technology, Vienna).